Acta Cryst. (1989). A**45**, 381-396

Statistical Theory of X-ray Scattering from Crystals of Finite Size with Pure Displacement Disorder in One Dimension*

BY MICHAEL SEUL

AT&T Bell Laboratories, 600 Mountain Avenue, Murray Hill, NJ 07974, USA

AND DAVID C. TORNEY

Theoretical Biology and Biophysics, Theoretical Divison, Group T-10, Mail Stop K710, Los Alamos National Laboratory, Los Alamos, NM 87545, USA

(*Received* 16 *August* 1988; *accepted* 13 *January* 1989)

Abstract

The statistical theory of X-ray scattering from a crystal that is disordered in one dimension is discussed. The state of disorder is characterized by probabilities that different types of scattering elements occupy specified positions. The effect this disorder has on the corresponding ensemble average axial reflections is determined. Finite size is explicitly accounted for. Motivated by recent experiments on water intercalation into thin, lyotropic multilayers, special consideration is given to systems whose components differ with respect to size, but not with respect to their scattering factors. Focusing on this case of pure displacement disorder in a binary mixture, a representation of the scattering function in closed form is derived. The case of a random binary mixture leads to the results of Hendricks & Teller [*J. Chem. Phys.* (1942), **10**, 147-167], and Méring [*Acta Cryst.* (1949), **2**, 371-377], while in the presence of nearest-neighbor correlations, a connection is established with the theory of Kakinoki & Komura [*J. Phys. Soc. Jpn* (1952), **7**, 30-35]. In extension of their treatment, systems with non-stationary transition probabilities are investigated. The effects on the scattering function of constraining composition fluctuations are also studied. Particular characteristics of the scattering function are displayed and discussed.

Glossary

Symbol and definition	Equation no.	Description
$\varphi_l = (2\pi/\lambda)(\hat{\mathbf{k}}_f - \hat{\mathbf{k}}_i)\cdot\mathbf{d}_l$	2	Phase of scattered X-rays from spacing of type l
$\mathbf{d}_l$	1*ff*	Vector normal to scattering plane with magnitude d_l, the thickness of spacing of type l
$\mathbf{l} = (\hat{\mathbf{k}}_f - \hat{\mathbf{k}}_i)d_1/\lambda$	above *B*.3*a*	Momentum transfer times d_1 over 2π
$W_n^j(k)$	3	Probability that in a substack of n spacings beginning with spacing k, exactly j spacings are type 1
$P_i(J)$	4	Probability that the ith spacing in a stack is type J
W_n^j	5	Probability that exactly j out of n spacings are type 1 given the first is chosen with the stationary probability
${}^1W_n^j$ (and ${}^2W_n^j$)	6	Probability that exactly j out of n spacings are type 1, given that the initial spacing is type 1 (type 2)
B_n	9, 11	Generating function of W_n^j
$B_n(k)$	32	Generating function of $W_n^j(k)$
$p = p_{11}$	4	Transition probability
$q = p_{22}$	4	Transition probability
$\mathbf{P} = \begin{pmatrix} p & 1-p \\ 1-q & q \end{pmatrix}$	4	Transition matrix
$E_1 = \exp(i\varphi_1)$	11	Complex exponential of phase of scattered X-rays
$E_2 = \exp(i\varphi_2)$	11	Complex exponential of phase of scattered X-rays
$\mathbf{Q} = \begin{pmatrix} E_1 & 0 \\ 0 & E_2 \end{pmatrix}\mathbf{P}$	11	
$f_1 = (1-q)/(2-p-q)$	11	Relative abundances
$f_2 = (1-p)/(2-p-q)$	11	Relative abundances
$\lambda = 1-p-q$	12	The negative of one eigenvalue of **P**
$\gamma = f_1E_1 + f_2E_2 = g\exp(-i\beta)$	12; *B*.2	
$\tau = \mathrm{trace}(\mathbf{Q}) = pE_1 + qE_2 = t\exp(-i\alpha)$	12; *B*.1	
$\Delta = \det(\mathbf{I}-\mathbf{Q}) = 1-\tau-E_1E_2$	27*ff*	

* Work supported by the US Department of Energy.

0108-7673/89/060381-16$03.00

1. Introduction

X-ray scattering from one-dimensionally disordered crystals was first considered theoretically by Landau (1937) and Lifschitz (1937, 1939). At about the same time, Hendricks & Teller (1942) interpreted experiments concerning the hydration of clay minerals. The analysis of this problem has been of central importance in the study of a wide range of structures, including interstratified clays (Reynolds, 1980), alloys (Guinier, 1958), face-centered cubic crystalts with deformation faults (Hosemann & Bagchi, 1954), and graphite intercalation compounds (Maire & Méring, 1970; Kim, Fischer, McWhan & Axe, 1986; Huster, Heiney, Cajipe & Fischer, 1987). In recent years it has been discussed in such diverse contexts as solid-state polymerization (Grimm, Axe & Kröhnke, 1982), charge-density wave stacking (Moncton, DiSalvo, Axe, Sham & Patton, 1976) and the hydration of chalcogenides (Johnston & Frysinger, 1984). Several theoretical descriptions have evolved subsequent to the work of Hendricks & Teller. These have been compared and discussed by Jagodzinski (1987), Welberry (1985), Kakinoki (1983) and Kakinoki & Komura (1952, 1965), who have developed a concise formulation employing transfer matrices. Motivated by recent experiments on water intercalation into thin lyotropic phospholipid multilayer films (Seul, 1988), we have examined in detail the analysis of X-ray scattering from a one-dimensionally disordered crystal of finite size. We have given special attention to linear systems containing two components that possess identical scattering factors but differ in size. When we refer to this situation as an incidence of pure displacement disorder, we mean to indicate its occurrence as a limiting case converse to that of pure substitution disorder, the latter referring to an alloy whose components are identical in size but differ in their scattering factors (Kakinoki & Komura, 1952; Guinier, 1963, §8). While we apply the term crystal to such disordered arrays, it must be borne in mind that this type of imperfection generally destroys long-range order (Guinier, 1963, §9).

Our analysis was motivated by attempts to develop an intuitive understanding of the characteristic lineshape of the scattering function for one-dimensionally disordered systems.

As with the aforementioned treatments of this problem, our theoretical analysis examines the ensemble average of the X-ray scattering intensity for probabilistically generated ensembles of stacks consisting of a finite number, N, of layers. Within this general framework we analyze the effect of various probabilistic rules on the ensemble average X-ray scattering intensity.

Each specific probabilistic rule dictating the construction of a stack corresponds to a state of disorder. Using generating functions, we derive the X-ray scattering function for the case of a binary mixture with pure displacement disorder and nearest-neighbor-layer correlations. In particular, we recover for the random layer sequence the well known results of Hendricks & Teller (1942) and Méring (1949). A direct connection with the theory of Kakinoki & Komura (1952, 1965) is established when applying their prescription, which is a stationary Markov chain with neighbor-dependent transition probabilities. Pertinent characteristics of the scattering function line shape are displayed and discussed. Here we are guided by recent experiments on water intercalation into thin lyotropic multilayers (Seul, 1988; Seul & Eisenberger, 1989). We examine both random and nearest-neighbor-correlated sequences and then turn to more general layer sequences characterised by position-dependent composition probabilities. Finally, we also investigate the effect of constraining fluctuations in layer composition.

2. General formulation

Consider a one-dimensional array, a *stack*, containing N planar layers. We discuss a system in which there are two possible *spacings*, the distances between the scattering planes in adjacent layers. The configuration of the spacings in the stack is specified by the vector $\mathbf{i}=(i_1, i_2, \ldots, i_{N-1})$, where $i_j \in \{1, 2\}$. The X-ray scattering intensity, I_N, from the stack is

$$I_N = \sum_{j=1}^{N} V_{i_j} \exp[i2\pi(\hat{\mathbf{k}}_f - \hat{\mathbf{k}}_i) \cdot \mathbf{r}_j/\lambda] \times \sum_{k=1}^{N} V_{i_k}^* \exp[-i2\pi(\hat{\mathbf{k}}_f - \hat{\mathbf{k}}_i) \cdot \mathbf{r}_k/\lambda]. \quad (1)$$

In (1), V_l is the form factor of a layer of composition l (James, 1982), and V_l^* is its complex conjugate; N is the number of layers; $\hat{\mathbf{k}}_i$ and $\hat{\mathbf{k}}_f$ are unit vectors in the directions of incidence and measurement; λ is the X-ray wavelength; and $\boldsymbol{r}_m$ is the position of the scattering plane of layer m. By rearranging the double summation in (1), it is seen that only the $N-1$ spacings between the scattering planes enter the scattering intensity. If we also define

$$\varphi_l \equiv 2\pi(\hat{\mathbf{k}}_f - \hat{\mathbf{k}}_i) \cdot \mathbf{d}_l/\lambda,$$

where $\mathbf{d}_l$ is a vector pointing along the normal to the stack with a magnitude equal to spacing l, (1) becomes

$$I_N = \sum_{j=1}^{N} |V_{i_j}|^2 + 2\,\mathrm{Re} \sum_{k>j=1}^{N} V_{i_j} V_{i_k}^* \times \exp[i\varphi_1(2k-2j-\sigma_{jk}) + i\varphi_2(\sigma_{jk}+j-k)], \quad (2)$$

with

$$\sigma_{jk} \equiv \sum_{l=j}^{k-1} i_l,$$

and the notation Re indicates that one takes the real part of the complex number. The factor multiplying φ_i is the number of spacings of type i in spacings j through $k-1$.

To obtain the ensemble average of I_N, $\langle I_N \rangle$, one sums the product of I_N for a given configuration and the probability of the corresponding configuration's occurrence over all possible configurations.

With pure *displacement disorder*, V_1 equals V_2 equals V, and (2) can be transformed to

$$\langle I_N \rangle / |V|^2 = N + 2\mathrm{Re} \sum_{n=1}^{N-1} \sum_{k=1}^{N-n} \sum_{j=0}^{n} W_n^j(k) \times \exp[i(j\varphi_1 + (n-j)\varphi_2)], \quad (3)$$

with $W_n^j(k)$ the probability that in the substack of n spacings beginning with spacing k, exactly j spacings are type 1. In this way, the probabilities that govern the construction of the stack are reflected in $\langle I_N \rangle$.

In the remainder of this section, we focus on nearest-neighbor-dependent transition probabilities (Bartlett, 1978). For our binary system this means that if the ith spacing has the probability $P_i(J)$ of being type J, the probability for the $(i+1)$th spacing is given by the matrix equation

$$(P_{i+1}(1), P_{i+1}(2)) = (P_i(1), P_i(2)) \begin{pmatrix} p & 1-p \\ 1-q & q \end{pmatrix}. \quad (4)$$

In (4), p and q are, respectively, the probabilities that a spacing of type 1 is followed by a spacing of type 1, and the probability that a spacing of type 2 is followed by a spacing of type 2.

Previous theories discuss the case where the first spacing is chosen with the probability

$$P_1(1) = (1-q)/(2-p-q), \quad (5)$$

the stationary abundance of type 1. Substitution of this probability on the right of (4) reveals that it generates an eigenvector of the matrix with eigenvalue 1. However, there is little additional difficulty in treating the more general situation where $P_1(1)$ is arbitrarily specified, as will be seen below. The advantage is that one can predict $\langle I_N \rangle$ for stacks with an independently specified initial spacing.

It is convenient to define two probabilities ${}^1W_n^j$ (and ${}^2W_n^j$) that are respectively the probabilites that exactly j out of n spacings are type 1, given that the initial spacing is type 1 (type 2). We have the following relationship with the $W_n^j(k)$ appearing in (3):

$$W_n^j(k) = P_k(1)\,{}^1W_n^j + P_k(2)\,{}^2W_n^j. \quad (6)$$

The advantage of this decomposition is that one has an explicit formula for $P_k(1)$, the probability that spacing k is type 1, as a function of p, q and $P_1(1)$ (Feller, 1968):

$$P_k(1) = \frac{1-q}{2-p-q} + \frac{(p+q-1)^{k-1}}{2-p-q} \times \{(1-p)P_1(1) - (1-q)[1-P_1(1)]\}. \quad (7)$$

This formula is derived using the eigenvectors and eigenvalues of the transition matrix in (4), the latter being 1 and $p+q-1$. Substitution of (6) and (7) into (3) allows the summation on k to be performed. The result is

$$\langle I_N \rangle / |V|^2 = N + 2\mathrm{Re} \sum_{n=1}^{N-1} \Bigg(\exp(in\varphi_2)(N-n) \times \sum_{j=0}^{n} W_n^j \exp[ij(\varphi_1 - \varphi_2)] + \{(1-p)P_1(1) - (1-q)[1-P_1(1)]\} \times [1-(p+q-1)^{N-n}] \times \sum_{j=0}^{n} ({}^1W_n^j - {}^2W_n^j) \exp[ij(\varphi_1 - \varphi_2)] \Bigg), \quad (8)$$

with W_n^j equal to the probability that exactly j out of n spacings are type 1, given that the first spacing is chosen with the probability shown by (5). Defining

$$B_n \equiv \sum_{j=0}^{n} W_n^j \exp\{i[j\varphi_1 + (n-j)\varphi_2]\}, \quad (9)$$

and using generating functions for the probabilities ${}^1W_n^j$ and ${}^2W_n^j$, we obtain the result

$$\langle I_N \rangle / |V|^2 = N + 2\,\mathrm{Re} \sum_{n=1}^{N-1} [(N-n)B_n + C_n], \quad (10a)$$

with

$$B_n = [(1-p)\exp(i\varphi_2) + (1-q)\exp(i\varphi_1)](\alpha_+^n - \alpha_-^n) \times [(2-p-q)(\alpha_+ - \alpha_-)]^{-1} + (1-p-q)\exp[i(\varphi_1+\varphi_2)](\alpha_+^{n-1} - \alpha_-^{n-1}) \times (\alpha_+ - \alpha_-)^{-1} \quad (10b)$$

and

$$C_n = \{(1-p)P_1(1) - (1-q)[1-P_1(1)]\} \times [(1-(p+q-1)^{N-n})/(2-p-q)^2] \times [\exp(i\varphi_1) - \exp(i\varphi_2)](\alpha_+^n - \alpha_-^n)/(\alpha_+ - \alpha_-), \quad (10c)$$

given that

$$\alpha_\pm = \tfrac{1}{2}(p\exp(i\varphi_1) + q\exp(i\varphi_2) \pm \{[p\exp(i\varphi_1) + q\exp(i\varphi_2)]^2 + 4(1-p-q)\exp[i(\varphi_1+\varphi_2)]\}^{1/2}). \quad (10d)$$

The derivation of these formulae is sketched in Appendix *A* and examined from a different vantage point in the next section.

For some applications, it may be of interest to perform the geometric summations in (10). Examples are discussed in later sections. In general, however, (10) suggests that peaks in $\langle I_N \rangle$ occur when α_+ or α_- are real. This point will be given further consideration in § 6. Unless explicitly stated otherwise, we assume the first spacing to be chosen according to (5) and therefore that C_n equals zero. Since C_n is the reflection of a constrained 'edge' spacing, $\langle I_N \rangle$ will ordinarily have its dominant contribution from the B_n.

3. Connection with Kakinoki & Komura's analysis

Kakinoki & Komura (1965) developed a transfer-matrix formalism for the numerical evaluation of the scattering intensity $\langle I_N \rangle$ that has been demonstrated to have wide applicability to the interpretation of scattering experiments on one-dimensionally disordered structures (Kakinoki, 1967; Komura & Kitano, 1977; Huster *et al.*, 1987; Seul, 1988). While generally not yielding a closed-form solution for $\langle I_N \rangle$, the theory is completely general insofar as it places no restrictions on the number of different components contributing to disorder or on the range of interlayer correlations. However, two important assumptions are made. These are, firstly, that the probabilistic rule to generate an ensemble of configurations may only be a Markov chain with stationary neighbor-dependent probabilities (Bartlett, 1978), and, secondly, that the first spacing may only be chosen at random; that is, its probability to be type 1 equals its stationary abundance.

In this section, we examine how the analysis given by Kakinoki & Komura (1965) and equivalent ones (Kakinoki, 1967, 1983) relate to our treatment. As expected, we establish that in the case of a binary crystal exhibiting pure displacement disorder with nearest-neighbor correlations, the theory of Kakinoki & Komura yields (10), if we take $C_n = 0$.

In subsequent sections, we will employ (3) to investigate more general probabilistic prescriptions for the construction of stacks and the resulting scattering functions. In the remainder of this section, we give an alternative derivation of (10*b*) by evaluating the B_n according to their definition as stated by Kakinoki & Komura (1965). Thus, the appropriate starting point is the expression

$$B_n = \text{trace}\left\{\begin{pmatrix}1 & 1\\ 1 & 1\end{pmatrix}\begin{pmatrix}f_1 & 0\\ 0 & f_2\end{pmatrix} \times\left[\begin{pmatrix}E_1 & 0\\ 0 & E_2\end{pmatrix}\begin{pmatrix}p & 1-p\\ 1-q & q\end{pmatrix}\right]^n\right\} \qquad (11a)$$

or

$$B_n = \text{trace}\left[\begin{pmatrix}f_1 & f_2\\ f_1 & f_2\end{pmatrix}\mathbf{Q}^n\right], \qquad (11b)$$

where $f_1 = (1-q)/(2-p-q)$ and $f_2 = (1-p)/(2-p-q)$ are stationary abundances of type 1 and type 2, respectively; $E_1 = \exp(i\varphi_1)$ and $E_2 = \exp(i\varphi_2)$. Note that f_1 is identical to $P_1(1)$ of (5). The transition matrix given in (4), which appears again on the right of (11), is denoted by **P**, while **Q** is defined to be the product of the matrix containing E_1 and E_2 with **P**.

First, we establish the representation

$$B_n = \gamma S_{n-1}(z)\tau^{n-1} + \lambda E_1 E_2 S_{n-2}(z)\tau^{n-2}, \qquad (12)$$

in terms of the combinatorial sums*

$$S_n(z) = \sum_{j=0}^{[n/2]} \binom{n-j}{j} z^j. \qquad (13)$$

In (12) and (13), we have introduced τ for trace (**Q**) and γ for $B_1 = f_1E_1 + f_2E_2$, while λ represents $1-p-q$, the negative of an eigenvalue of the transition matrix **P**. Equation (12) will be shown to hold for a particular choice of the variable z.

To obtain (12), we begin by casting **Q** in the form

$$\mathbf{Q} = \begin{pmatrix}pE_1 & qE_1\\ pE_2 & qE_2\end{pmatrix} + \lambda\begin{pmatrix}0 & E_1\\ E_2 & 0\end{pmatrix} \qquad (14)$$

from which it is readily established that

$$\mathbf{Q}^n = \eta_n\mathbf{Q} + \kappa_n\mathbf{I}. \qquad (15)$$

Complete induction on (15) yields the recursion relations satisfied by the η_n and κ_n:

$$\eta_{m+1} = \eta_m\tau + \eta_{m-1}\lambda E_1E_2 \qquad (16a)$$

$$\kappa_{m+1} = \eta_m\lambda E_1E_2. \qquad (16b)$$

Equations (16) hold for $m \geq 2$ with $\eta_1 = 1$, $\eta_2 = \tau$, and $\kappa_1 = 1$. Combining (11*b*), (15) and (16), we find

$$B_n = \eta_n\gamma + \eta_{n-1}\lambda E_1E_2, \qquad (17)$$

and, by employing (16), a useful recursion relation for B_n:

$$B_n = \tau B_{n-1} + \lambda E_1E_2B_{n-2}, \qquad (18)$$

valid for $n \geq 2$, with $B_0 = 1$ and $B_1 = \gamma$. As before, $\tau = \text{trace}(\mathbf{Q}) = pE_1 + qE_2$. The iteration of (18) immediately yields (12), if we let $z = \lambda E_1E_2/\tau^2$.

---

* We note that $S_n(z)$ is the hypergeometric function, ${}_1F_0(a; z)$, with $a = n-2j+1$:

$$S_n(z) = \sum_{j=0}^{[n/2]} (n-2j+1)_j(z^j/j!) \equiv {}_1F_0(n-2j+1; z),$$

where, for any $k \in R$, $(k)_j = k(k+1)\ldots(k+j-1)$ (*e.g.* Slater, 1960).

Next, we establish the identity

$$S_n(z)=\frac{(1+\delta)^{n+1}-(1-\delta)^{n+1}}{2^n[(1+\delta)-(1-\delta)]} \tag{19}$$

for the sum defined in (13). Here,

$$\delta=(1+4\lambda E_1E_2/\tau^2)^{1/2}.$$

To obtain (19), note that the recursion relation for the B_n implies a similar identity for the S_n by virtue of (12). Thus

$$S_n(z)=S_{n-1}(z)+zS_{n-2}(z). \tag{20}$$

The generating function, $T(z,\tau)\equiv\sum_{n=0}^{\infty}S_n(z)\tau^n$, then satisfies the identity

$$T(z,\tau)=(1-\tau-z\tau^2)^{-1}, \tag{21}$$

as follows readily from (20). Partial-fraction expansion of (21) (see also Riordan, 1968; problem 7 of ch. 2) leads to (19).

Noting that in terms of the notation introduced in this section, $\alpha_\pm$ of (10) may be written in the form

$$\alpha_\pm=\tfrac{1}{2}\tau(1\pm\delta), \tag{22}$$

we may combine (12) and (19) to obtain the expression for the B_n given in (10*b*):

$$B_n=\gamma\frac{\alpha_+^n-\alpha_-^n}{\alpha_+-\alpha_-}+\lambda E_1E_2\frac{\alpha_+^{n-1}-\alpha_-^{n-1}}{\alpha_+-\alpha_-}. \tag{23}$$

4. Special cases

In the following three limiting cases the B_n have a particularly simple form.

(*a*) *Perfect superlattice ordering*

$p\to 0$, $q\to 0$: $f_1=f_2=\frac{1}{2}$ and $\lambda=1$, $\tau=0$. Then for $n\geq 2$, $B_n=B_{n-2}E_1E_2$, leading to

$$B_{2n}^{S.L}=(E_1E_2)^n \tag{24a}$$

$$B_{2n+1}^{S.L}=\tfrac{1}{2}(E_1+E_2)(E_1E_2)^n. \tag{24b}$$

(*b*) *Complete segregation*

$p\to 1$, $q\to 1$: here we have $\lambda\to 1$, $\tau\to E_1+E_2$. From (18), $B_n=B_{n-1}(E_1+E_2)-B_{n-2}E_1E_2$, for $n\geq 2$. It readily follows by induction that

$$B_n^{CS}=f_1E_1^n+f_2E_2^n. \tag{24c}$$

(*c*) *Random stacking*

$p=1-q=f_1$, $q=1-p=f_2$: since $\lambda=0$, we have $B_n=\tau B_{n-1}$, and, with $B_0=1$,

$$B_n^{RS}=\tau^n. \tag{24d}$$

The W_n^j are binomial in this case.

5. Finite system size

Following Kakinoki & Komura, the contributions from B_n to $\langle I_N\rangle$ may be divided into two parts, given a non-vanishing determinant of $\mathbf{I}-\mathbf{Q}$, $\mathbf{I}$ being the identity matrix:

$$\langle I_N\rangle/|V|^2=ND+H. \tag{25}$$

Performing the geometric series, (10*a*), to evaluate $\langle I_N\rangle$, using (10*b*) or (23) for B_n, and collecting terms multiplied by N gives

$$D=1+2\mathrm{Re}[(\lambda E_1E_2+\gamma)/(1-\alpha_+)(1-\alpha_-)], \tag{26}$$

and the remaining terms comprise H:

$$\begin{aligned}H=2\mathrm{Re}\{&(\alpha_+-\alpha_-)^{-1}\\&\times[(\alpha_+^N-1)(1-\alpha_+)^{-2}(\alpha_+\gamma+\lambda E_1E_2)\\&-(\alpha_-^N-1)(1-\alpha_-)^{-2}(\alpha_-\gamma+\lambda E_1E_2)]\}.\end{aligned} \tag{27}$$

H has an additional term, from (10*c*), if the C_n are not equal to zero. Note that D is independent of N; whereas, so long as neither α_+ nor α_- equal unity, H is bounded and has some residual N dependence and a finite limit as N goes to infinity. The value of N for which it is a reasonable approximation to discard H is a function of the parameters p, q, φ_1 and φ_2, as can be ascertained from subsequent figures. Generally, it is clear that, when the limit exists, D is defined to be the limit of $\langle I_N\rangle/N$ as N goes to infinity and H is defined to be $\langle I_N\rangle-ND$.

We also note that

$$H=-2\mathrm{Re}\left\{(1/\Delta)\sum_{n=1}^{N}[(1-\tau)B_n+B_{1+n}]\right\}$$

[Kakinoki & Komura (1965); their equation (36)]. Here, Δ denotes the determinant of $\mathbf{I}-\mathbf{Q}$, given by $\Delta=1-\tau-\lambda E_1E_2$. Defining the summand of the latter equation to be H_n, the recursion relation, (18), immediately yields

$$H_n=\tau H_{n-1}+\lambda E_1E_2H_{n-2},$$

valid for $n\geq 2$ with

$$H_0\equiv -2\mathrm{Re}[(1/\Delta)(1-\tau+\gamma)]$$

$$H_1\equiv -2\mathrm{Re}[(1/\Delta)(\gamma+\lambda E_1E_2)].$$

In the remainder of this section we show that the equations given by Hendricks & Teller (1942) and Méring (1949) for D and H, respectively, for a random stack can be obtained from (26) and (27). In the random stacking limit, $\alpha_+=\tau$ and $\alpha_-=0$. In Appendix *B* a polar representation is introduced for the complex quantitites appearing in (26) and (27), and it follows from (*B*.3) with $\tau=\gamma$, $\lambda=0$ that

$$D^{RS}=\frac{1-t^2}{1-2t\cos\alpha+t^2}, \tag{28}$$

where $\tau=t\exp(-i\alpha)$, as detailed in Appendix *B*. In

the random stacking limit, t of ($B.1b$) assumes the form

$$t=[1-4p(1-p)\sin^2\tfrac{1}{2}(\varphi_1-\varphi_2)]^{1/2}. \qquad (29)$$

Méring (1949) was the first to take proper account of finite size effects in the randomly stacked layers. Employing the polar representation introduced in Appendix B, we obtain

$$H^{RS}=\{2t[2t-(1+t^2)\cos\alpha][1-t^N\cos(N\alpha)] -2t^{N+1}\sin(N\alpha)(1-t^2)\sin\alpha\} \times(1-2t\cos\alpha+t^2)^{-2}. \qquad (30)$$

As pointed out by Méring, the Laue function is recovered from H^{RS} in the limit $t\to 1$.

6. Characteristic features of the scattering function

The scattering function for a binary stack of N layers with nearest-neighbor correlated spacings exhibits characteristic features determined by the transition probabilities p and q. In this section we show how the lineshape, described by such attributes as line width, peak position, asymmetry, and peak separation, evolves as p and q are systematically varied thoughout the range $0\le p, q\le 1$. Emerging trends are discussed in light of the previously derived results. We focus first on systems with p and q independent of position. We then extend our considerations to position-dependent probabilities.

We refer in what follows to parameter space, illustrated in Fig. 1. As is apparent, the regions of superlattice ordering and segregation share as a common boundary the diagonal $2-p-q=1$, the locus of all possible random stacking sequences. The reflection symmetry of the map about the diagonal $p=q$, the locus of equi-abundant sequences, is a consequence of the symmetry of the generating function B_n of (9) and (10) with respect to interchanging p and q. The

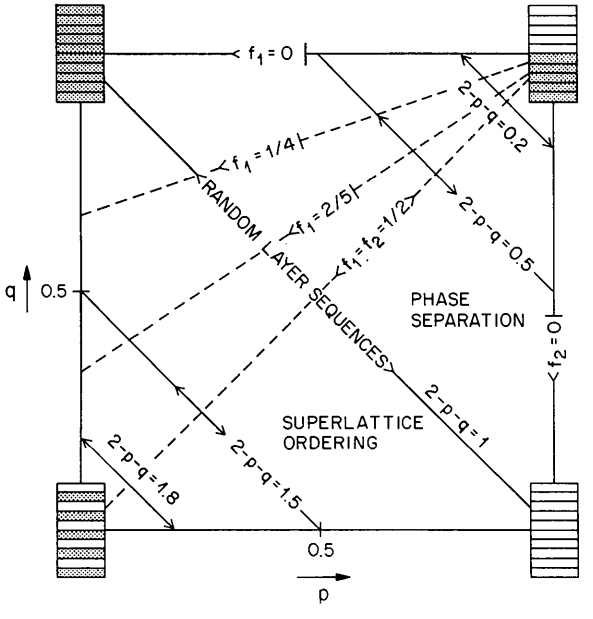

Fig. 1. Parameter-space map of the nearest-neighbor correlated stacking model, spanned by $p=p_{11}$, the probability that type 1 follows type 1 and $q=p_{22}$, the probability that type 2 follows type 2. The relative abundances are $f_1=(1-q)/(1-p-q)$ and $f_2=(1-p)/(2-p-q)=1-f_1$. Phase separation, or segregation, occurs for $2-p-q<1$, *i.e.* in the upper right triangle; superlattice ordering, leading to alternating layer sequences, is favored for $(2-p-q)>1$, *i.e.* in the lower left triangle. The locus of all random stacking sequences is the diagonal $2-p-q=1=p+q$, connecting the two pure states. The loci of constant composition f_1 are straight lines of form $1=[f_1/(1-f_1)]p+(1-2f_1)/(1-f_1)$, some of which are indicated. The upper and right edges represent the loci of pure states 2 and 1, respectively. All lines of constant composition end in the neighborhood of the point $p=q=1$. This point itself, however, is included only by the diagonal $p=q$, the locus of equi-abundant sequences. Note the reflection symmetry of the map with respect to this line.

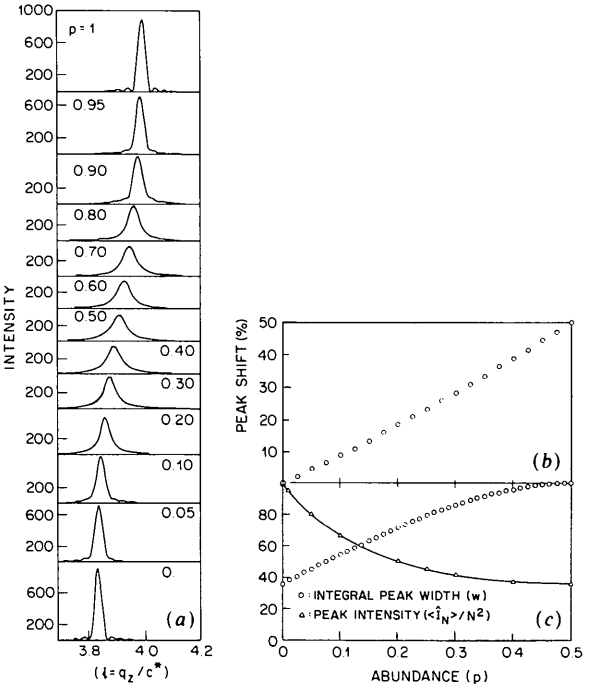

Fig. 2. Random layer sequences, $p=f_1$, $q=f_2=1-p$. (a) The evolution of line shapes (for the 004 maximum) as the composition is varied along the diagonal $q=1-p$. Each pure state exhibits a Laue function (top and bottom panels). Here, $c^*=2\pi/d_1$. (b) and (c) show how peak shift as well as peak height and integral peak width depend on p. In (b), relative peak displacements between the two pure states are shown. In (c), peak heights have been normalized to that of the pure state. The solid line representing the peak height as a function of p is an exact representation, obtained from equation (31) in the text. The integral peak width plotted here is the normalized quantity $w/w(p=0{\cdot}5)$, where w is defined in the text. The graphs in (c) are mirror-symmetric with respect to the line $p=0{\cdot}5$. For the example shown here, *i.e.* $N=30$, $d_1=56{\cdot}5$ and $d_2=58{\cdot}9$ Å, the integral width of the 004 harmonic increases approximately threefold between pure ($p=0$) and equi-abundant ($p=0{\cdot}5$) states.

loci of constant composition are straight lines ending at the point (1, 1).

6.0. *Random stacking sequences*

We start by giving detailed consideration to random stacking, where $q = 1 - p$. As p is varied from 0 to 0·5, the composition of a stack changes linearly from pure type 2 (upper left-hand corner of map) to equal abundance of types 1 and 2 (center of map). Fig. 2(a) illustrates the evolution of the line shape. Figs. 2(b) and (c) summarize the composition dependence of the line width and the peak intensity.

From the observation made in connection with (24d), namely that in the random stacking limit B_n is the generating function for the binomial distribution, the approximate linear peak shift may be attributed to the linear composition dependence of the mean of that distribution.

To discuss the behavior of the line width, we first define the integral peak width in the usual way (Guinier, 1963), *i.e.*

$$w \equiv I_\Sigma / \langle \hat{I}_N \rangle,$$

where I_Σ and $\langle \hat{I}_N \rangle$ represent the integrated and the peak intensity, respectively. If we let $\tilde{l}$ denote a suitable range of integration, *e.g.* the period set by $d_1/(d_2 - d_1)$, I_Σ may be defined as

$$I_\Sigma = (1/\tilde{l}) \int_0^{\tilde{l}} \langle I_N \rangle \mathrm{d}l.$$

I_Σ is of order N, independent of composition. This result holds for all stacking sequences in the limit of pure displacement disorder.*

The peak position is found from the condition that all B_n are real, so that $\exp(-in\alpha) = 1$, or $\alpha = 0, 2\pi, 4\pi, \ldots$. Hence, from (24$d$), (10) reads:

$$\langle \hat{I}_N \rangle = N + 2 \sum_{n=1}^{N-1} (N-n) t^n,$$

which may be evaluated without difficulty to yield

$$\langle \hat{I}_N \rangle = [N(1-t^2) - 2t + 2t^{N+1}](1-t)^{-2}. \quad (31)$$

As expected, in the pure state, $\langle \hat{I}_N \rangle$ is of order N^2. This is verified by expanding $\langle \hat{I}_N \rangle$ in terms of $\varepsilon = 1 - t$, yielding $\langle \hat{I}_N \rangle \doteq N^2[1 - (N/3)\varepsilon]$, provided $1 \gg N\varepsilon$ or

* This follows from the evaluation of the integral

$$(1/\tilde{l}) \int_0^{\tilde{l}} 2\mathrm{Re}\{B_n\} \, \mathrm{d}l,$$

which is readily accomplished by recourse to the representation of B_n given in (9). The resulting integral,

$$(2/\tilde{l}) \int_0^{\tilde{l}} \cos \varphi_1 [j + x(n-j)] \, \mathrm{d}l,$$

with $x = \varphi_2/\varphi_1$, is of the order $1/\tilde{l}$ and can thus be made arbitrarily small. Hence, the only contribution to I_Σ is of order N, resulting from the constant term in (10).

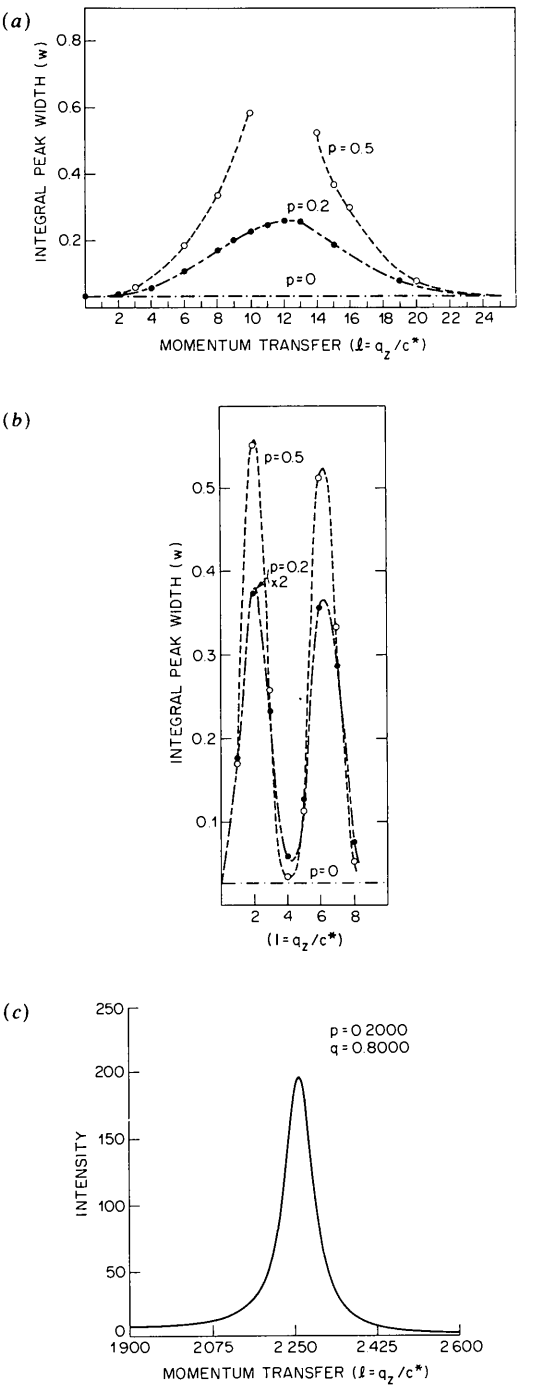

Fig. 3. Random stacking. Dependence of integral peak width of the 004 harmonic on momentum transfer $l = q_z/c^*$, where $c^* = 2\pi/d_1$. In (a), $N = 30$, $d_1 = 56{\cdot}5$ and $d_2 = 58{\cdot}9$ Å, parameters relevant to phospholipid multilayers (Suel, 1988). In (b), $N = 30$, $d_1 = 9{\cdot}045$ and $d_2 = 11{\cdot}85$ Å, spacings encountered in a study of $Na_{1/3}(H_2O)_yTaS_2$ (Johnston & Frysinger, 1984). (c) The line shape of the 003 peak, with $p = 0{\cdot}2$, an example of a random stack generating an asymmetric line shape. In both (a) and (b), values of w near the maxima of the curves for $p = 0{\cdot}5$ are ill defined due to substantial overlap of adjacent harmonics; the corresponding points have therefore been omitted. Lines are guides to the eye.

$t \gg 1-(1/N)$. The solid line through the points $[p, \langle \hat{I}_N \rangle]$ (see Fig. 2*c*) is obtained by evaluating $\langle \hat{I}_N \rangle$ of (31), using t at the peak position as obtained from (29).

The dependence of w and $\langle \hat{I}_N \rangle$ on the order of the harmonic, numbered by the index l, is shown in Fig. 3. The functional form follows immediately from (31) by way of the l dependence of t, recalling the definition of w. The oscillatory l dependence of w is a hallmark of Hendricks-Teller type disorder (*e.g.* Johnston & Frysinger, 1984; Seul & Eisenberger, 1989). It may be rationalized as the result of the 'beating' of the two spatial frequencies, φ_1 and $\varphi_2 > \varphi_1$. The corresponding beat frequency is set by the condition $(l+1)\varphi_1 = l\varphi_2$, or, using the representation of t in (29), by the condition $\sin^2 \frac{1}{2}(\varphi_1 - \varphi_2) = 1$. This leads to $l 2\pi/d_1 = (l+1)2\pi/d_2$, or $l = d_1/(d_2 - d_1)$, thus determining the period of the oscillation. For the two examples shown in Figs. 3(*a*) and (*b*), we obtain respectively $d_1/(d_2 - d_1) \doteq 24$ and $d_1/(d_2 - d_1) \doteq 4$. It is important to note that the dependence of w on l contains information about the relative abundance of components, which determines the amplitude, $t_{\max} = 1 - 4p(1-p)$, as well as the difference in their spacings - which determines the period of the oscillation. This is a valuable tool for the analysis of experimental data. If this oscillation is slow, as depicted in Fig. 3(*a*), the line shapes appear symmetric. This follows as long as the modulus t^n of $B_n = t^n \exp(-in\alpha)$ varies slowly over the width of a given peak. The phase factor of B_n, $2\cos n\alpha$, is of course always symmetric with respect to $\alpha = 0, 2\pi, 4\pi, \ldots$. Under most conditions, the line-shape asymmetry is not expected to exceed the extent illustrated in the example displayed in Fig. 3(*c*). Fig. 4 displays the dependence on system size of the integral peak width of several harmonics and documents noticeable finite size effects up to at least $N = 50$.

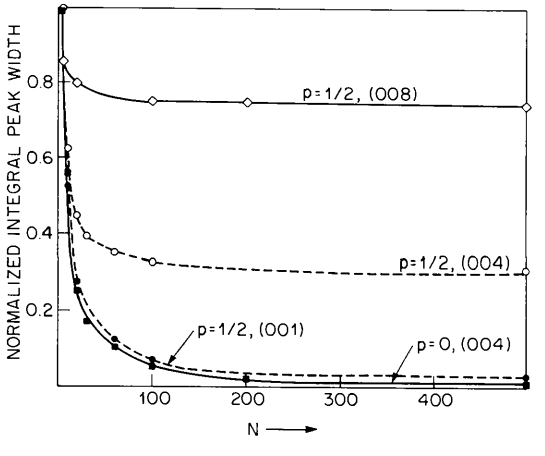

Fig. 4. Random stacking. The evolution of the integral peak width (normalized to that of a five-layer stack) with system size is displayed for the 001, 004 and 008 peaks in an equi-abundant ($p = 0{\cdot}5$), and for the 004 peak in a pure ($p = 0$) system. Finite-size effects are noticeable up to at least $N = 50$. In these examples, $d_1 = 56{\cdot}5$, $d_2 = 58{\cdot}9$Å.

6.1. *Nearest-neighbor correlated stacking with stationary transition probabilities*

In discussing correlated stacking sequences, it is natural to distinguish the regimes of segregation, located in the upper right triangle of the map exhibited in Fig. 1, and of superlattice ordering, in the lower left triangle. In the former, layers of equal type attract one another, while in the latter they repel. The analogy to ferromagnetic and antiferromagnetic ordering of the one-dimensional Ising model may be called upon to provide a physical interpretation of the transition probabilities, p_{ij}. This is suitably accomplished by inspection of the transfer matrix describing the Ising chain (*e.g.* Huang, 1963):

$$P^{\text{Ising}} = \begin{pmatrix} \exp[\beta(j+h)] & \exp(-\beta j) \\ \exp(-\beta j) & \exp[\beta(j-h)] \end{pmatrix}.$$

Here j denotes the exchange interaction and h an externally applied magnetic field while, as usual, $\beta = 1/kT$. The matrix elements represent the statistical weights assigned according to a Boltzmann distribution to the occurrence in the chain of spin pairs of the form ↑↑, ↓↓, ↑↓ and ↓↑. These weights correspond in the system under consideration to the probability densities, n_{ij}, of the four possible types of junctions. These are: $n_{11} = f_1 p$, $n_{22} = f_2 q$, $n_{12} = f_1(1-p)$, and $n_{21} = f_2(1-q) = n_{12}$. As usual, the chain is made cyclic by including a junction between the last and the first layer. We thus have the following correspondences:

$$f_1 p \simeq (1/S)\exp[\beta(j+h)]$$

$$f_2 q \simeq (1/S)\exp[\beta(j-h)]$$

$$f_1(1-p) = f_2(1-q) \simeq (1/S)\exp(-\beta j),$$

where $S = \exp[\beta(j+h)] + \exp[\beta(j-h)] + 2\exp(-\beta j)$. The strength of the applied magnetic field determines the magnetization, *i.e.* the abundance of the two types of spins in the Ising chain. That is,

$$\frac{n_{11}n_{21}}{n_{12}n_{22}} = \frac{p}{(1-p)}\,\frac{(1-q)}{q} \simeq \exp(-2\beta h).$$

The exchange interaction directly corresponds to the specified strength of interlayer correlations. Thus (*e.g.* Kasteleyn, 1971),

$$\frac{n_{11}n_{22}}{n_{12}n_{21}} = \frac{p}{1-p}\,\frac{q}{1-q} \simeq \exp(4\beta j).$$

This quantity diverges in the ferromagnetic limit, $j > 0$, $T \to 0$, or $p \to 1$, $q \to 1$. The number of junctions between identical types of layers approaches $f_1 N$ or $f_2 N$ and diverges with $N \to \infty$. In the antiferromagnetic limit, $j < 0$, $T \to 0$, or $p \to 0$, $q \to 0$, analogous conclusions hold for the number of junctions between

different types of layers. The random stacking limit is seen to correspond to setting $j=0$: the quantity $n_{11}n_{22}/n_{12}n_{21}$ equals unity. In this limit, the length of substacks of pure component 1 or 2, *i.e.* the cluster size, approaches N as p or q approach unity.

According to (10) the scattering function, $\langle I_N \rangle$, for nearest-neighbor correlated sequences of a binary stack of N layers is determined by two eigenvalues, $\alpha_\pm$. In the foregoing, the discussion of random stacking already profited from the inspection of the roots of Im (α_+), the single non-trivial eigenvalue in that limit. Indeed, a favorable approach to the exposition of the salient features exhibited by $\langle I_N \rangle$ throughout the range $0 \leq p,\ q \leq 1$ is suggested by consideration of the roots of the imaginary part of both α_+ and α_-. In this general case, contributions to $\langle I_N \rangle$ arise from both α_+ and α_- and the line shape of $\langle I_N \rangle$ must reflect the presence of two components, Re (α_+) and Re (α_-) evaluated at positions of vanishing Im (α_+) and Im (α_-).

In Fig. 5(a) we have plotted Im(α_+) and Im(α_-) *versus* momentum transfer, for particular choices of d_1, d_2 and N, evaluating functions for a number of points along the diagonal $p = q$ of the parameter space of Fig. 1. Importantly, the node positions remain essentially unchanged for $0 \leq p \leq 0{\cdot}5$, while finite separations evolve in the regime of segregation, specifically for $p \geq 0{\cdot}6$. Implications for the actual line shapes may be ascertained from Fig. 5(b), which documents for the 004 peak the eventual evolution of two resolved peaks in the regime of segregation.

Fig. 6 displays the behavior of the node separation throughout parameter space. Note that we have chosen to display the absolute value of the separation, rather than the separation itself, to obtain a surface that is *symmetric* rather than antisymmetric with respect to the line $p = q$.

Asymmetric line shapes are expected when $p \neq q$, reflecting unequal contributions of α_+ and α_-. A representative sample of shapes is displayed in Figs. 7 and 8.

6.2. *Random stacking with position-dependent abundance*

We now extend the discussion of the previous section to stacking sequences characterized by a position-dependent composition, focusing attention on the random stacking limit. In the context of the previously discussed one-dimensional Ising model, this situation corresponds to the application of a spatially varying magnetic field to the disordered phase.

We treat this problem on the basis of the general formulation of § 2. Equation (3) represents a

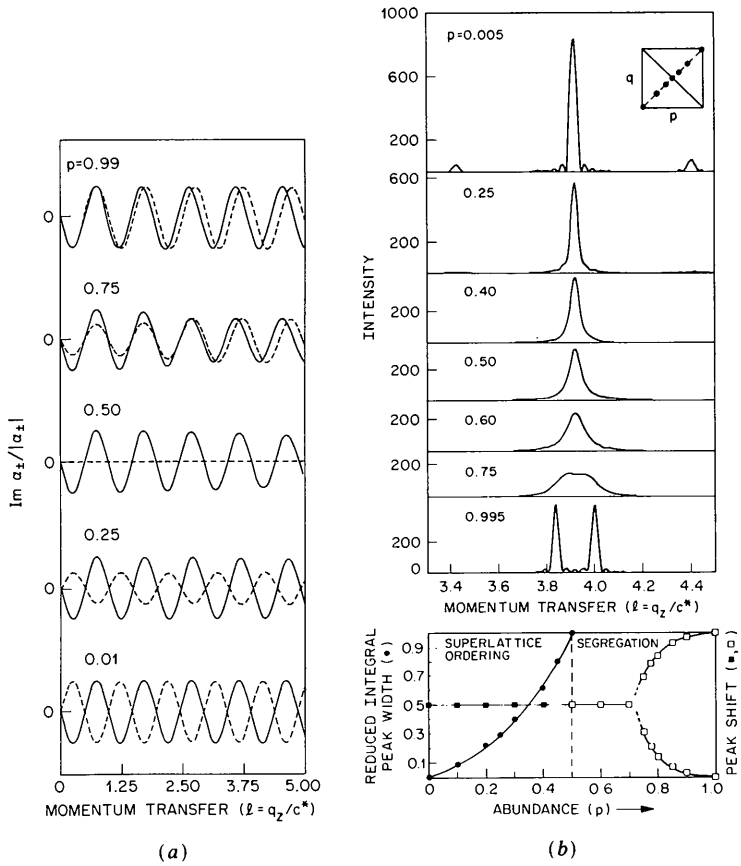

Fig. 5. Nearest-neighbor correlated stacking. (a) The behavior of Im (α_+) and Im (α_-) of equation (10) of the text along the diagonal $p = q$. The roots of these functions mark all possible peak positions. In the example, $N = 30$, $d_2/d_1 = 1{\cdot}04278$. (b) The evolution of the 004 line shape along the line $p = q$. Here, $d_1 = 56{\cdot}5$ and $d_2 = 58{\cdot}9$ Å. Two resolved peaks in the segregation regime merge as p and q decrease; in the limit of superlattice ordering, a Laue peak with secondary maxima emerges. The inset in the top panel of (b) shows the position of the displayed scans in the parameter-space map of Fig. 1. The bottom panel in (b) summarizes the behavior of integral peak width, $\tilde{w}$, and peak shifts, $\tilde{q}$. The reduced quantities plotted here are defined as follows: $\tilde{w} = [w(p) - w(p=0)]/[w(p=0{\cdot}5) - w(p=0)]$ and $\tilde{q} = (\hat{q} - \hat{q}_2)/(\hat{q}_2 - \hat{q}_1)$, where $\hat{q}$ indicates a peak position, *i.e.* $\hat{q}_1 = 2\pi/d_1$ and $\hat{q}_2 = 2\pi/d_2$. Here, solid lines are guides to the eye.

convenient starting point because it contains a position-dependent probability distribution, $W_n^j(k)$. The corresponding position-dependent generating function $B_n(k)$ is defined in analogy to (9) as

$$B_n(k) \equiv \exp(in\varphi_2) \sum_{j=0}^{n} W_n^j(k) \exp[ij(\varphi_1 - \varphi_2)], \quad (32)$$

and, with reference to (3),

$$\langle I_N \rangle / |V|^2 = N + 2 \operatorname{Re} \sum_{n=1}^{N-1} \sum_{k=1}^{N-n} B_n(k).$$

The absence of correlations permits us to rewrite $B_n(k)$ as a product of the probabilities, $f(j)$, that spacing j is type 1. Thus,

$$B_n(k) = \prod_{j=k}^{k+n-1} \{f(j) \exp(i\varphi_1) + [1 - f(j)] \exp(i\varphi_2)\}. \quad (33)$$

Although we have not investigated the full range of possibilities of this model, we have evaluated the scattering function given above with $B_n(k)$ of (33) using three functional forms for the position dependence of f, an exponential, a step and a Gaussian profile. To compute the $B_n(k)$, we start with the $B_{N-1}(1)$ from which we generate $B_{N-2}(1)$ and $B_{N-2}(2)$ *etc.*, minimizing the number of multiplications and divisions. The resulting computation is efficient and requires of the order of N^2 operations to compute I_N; a Fortran program is included as Appendix C.

To facilitate a meaningful extrapolation from the case of stationary transition probabilities discussed above to the cases under consideration here, the parameters defining each profile are constrained in such a way that the resulting sequences yield the same average abundance. That is, for a set of specified parameters, the different profiles generate stacks of identical average composition which differ only in their spatial distribution of the available layers of type 1 and type 2. The three profiles of interest specify the abundance at position k in the stack as follows ($0 \le k \le N-1$):

$$f(k) = f(0) \exp(-k/\lambda) \quad (34a)$$

$$f(k) = f(0) \exp(-k^2/\sigma^2) \quad (34b)$$

$$f(k) = f(0) H(l - k). \quad (34c)$$

Here, $f(0)$ is the probability that the first layer is of type 1; in (34c), H denotes a step function, *i.e.* $H(j) = 0$ for $j \le 0$, $H(j) = 1$ otherwise. Defining an average

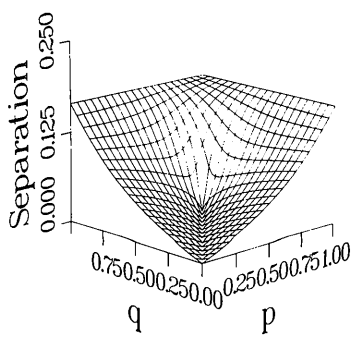

Fig. 6. Nearest-neighbor correlated stacking. We display the separation (in units of $2\pi/d_1$) of the roots of $\mathrm{Im}(\alpha_+)$ and $\mathrm{Im}(\alpha_-)$ for the 004 peak. Calculations were based on an example with $N = 30$, $d_1 = 56{\cdot}5$ and $d_2 = 58{\cdot}9$ Å. The topography of the surfaces for other Bragg peaks is identical - the separation scaling, however, with the order of the harmonic [up to $\tilde{l} = d_1/(d_2 - d_1)$; see text]. To obtain a surface displaying reflection rather than inversion symmetry with respect to the line $p = q$, we have plotted the absolute value of the separation.

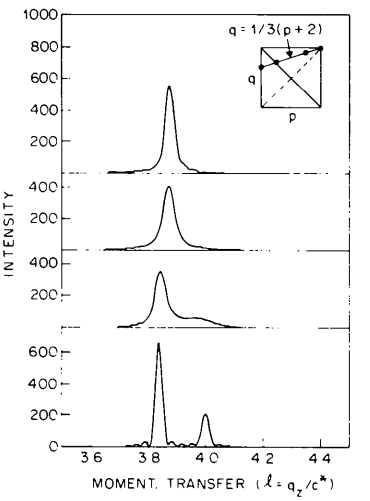

(a)

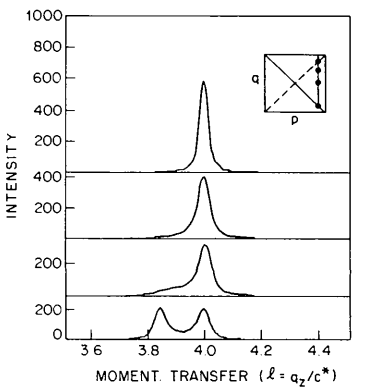

(b)

Fig. 7. Nearest-neighbor correlated stacking. Examples of typical line shapes, here for a 004 peak of a system described by parameters $N = 30$, $d_1 = 56{\cdot}5$ and $d_2 = 58{\cdot}9$ Å. The loci corresponding to the line shapes are indicated in the insets, which refer to the parameter-space map of Fig. 1. Plots along the following diagonals are shown. In (*a*): $2 - p - q = 1{\cdot}5$; in (*b*): $2 - p - q = 0{\cdot}5$.

composition $\bar{f}$ as

$$\bar{f}=(1/N)\sum_{k=0}^{N-1} f(k), \tag{35}$$

we obtain for the exponential profile

$$\bar{f}=(1/N)f(0)S_N(\lambda), \tag{36a}$$

where

$$S_N(\lambda)=\frac{1-\exp(-N/\lambda)}{1-\exp(-1/\lambda)}. \tag{36b}$$

We now determine σ for the Gaussian and l for the step profile such that $\bar{f}$ is identical for all three profiles. For the Gaussian, σ was determined numerically from the condition

$$\sum_{k=0}^{N-1}\exp(-k^2/\sigma^2)=S_N(\lambda). \tag{37}$$

For the step profile, l follows from the condition

$$f(0)l+[(N-1)-l]f(0)\exp[-(N-1)/\lambda]=S_N(\lambda). \tag{38}$$

Each profile is thus characterized by *two* parameters: an amplitude, $f(0)$, common to all of them, and a decay length, specified for the exponential, and then determined by virtue of (37) and (38) for the Gaussian and the step profile.

The introduction of a position-dependent abundance in the form of the profiles of (34) in a random stacking sequence leads to partial or complete segregation. As a result, random stacking sequences with position-dependent abundance are displaced in phase space with respect to the corresponding stationary sequence of equal *average* composition toward the regime of segregation, *i.e.* the upper right triangle of Fig. 1. The step profile causes the largest displacement because its inherent two-state nature favors complete segregation. Qualitatively, random layer sequences with position-dependent abundances closely resemble the binary nearest-neighbor correlated stacking models with stationary transition probabilities.

While there exists this qualitative similarity, we note that most sequences generated by both Gaussian and exponential abundance profiles cannot be duplicated by a binary correlated stacking model. The reason lies in the fact that the new line shapes no longer have a representation in terms of only two complex eigenvalues, $\alpha_\pm$ of (10). As a result, the line shapes acquire characteristic features such as those

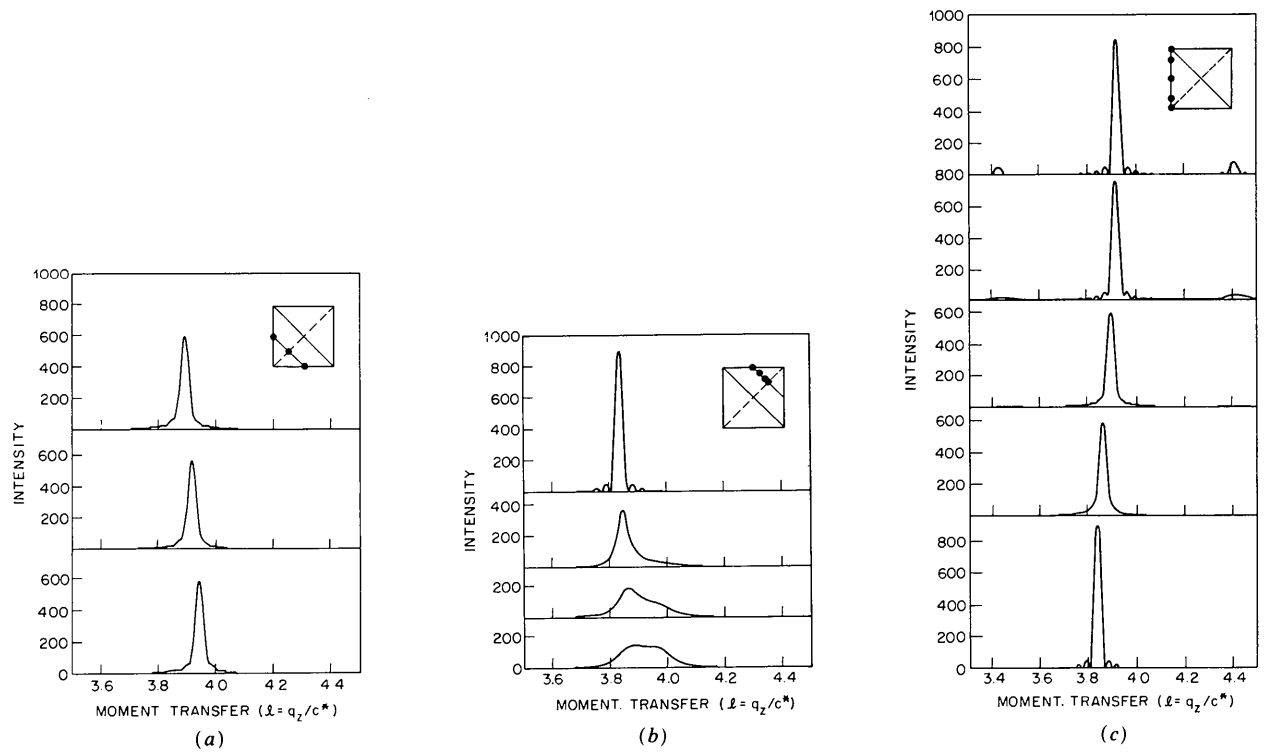

Fig. 8. Nearest-neighbor correlated stacking. More examples of typical line shapes. Parameters are as before; the loci in the parameter-space map are indicated in the insets. Specifically, plots along the following straight lines are shown. In (*a*): $q=\frac{1}{3}(p+2)$, a line of constant composition with $f_1=\frac{1}{4}$, $f_2=\frac{3}{4}$. Actual profiles are drawn for ($p=0$, $q=0{\cdot}67$), ($0{\cdot}25$, $0{\cdot}75$), ($0{\cdot}75$, $0{\cdot}417$) and ($0{\cdot}99$, $0{\cdot}997$), from top to bottom. In (*b*): $p=0{\cdot}9$; in (*c*): $p=0$.

displayed in Figs. 10 and 11. The applicability of a random stacking model with exponential position dependence has been recently demonstrated in the analysis of X-ray scattering data obtained on thin substrate-deposited lyotropic multilayers. It is interpreted as a consequence of an inhomogeneous distribution of hydrated states throughout the multilayer (Seul & Eisenberger, 1989).

The presentation of the parameter space map of the Gaussian composition profile depicted in Fig. 9 is chosen to indicate this close relationship with the map of Fig. 1: the $\bar{f}$ axis corresponds to the diagonal $p = 1 - q$ in that figure. The map exhibits contours of constant decay length, λ. The form of the dependence of $\bar{f}$ on λ is given by (36). For given $\bar{f}$, the tendency toward phase separation is noticeably weaker for the exponential profile as compared with the step profile. The Gaussian profile is seen to be intermediate between exponential and step profiles in effecting enhanced segregation. This is apparent from the series of model line shapes generated at constant $f(0)$ and plotted in Fig. 10 to illustrate the effect of an increasing decay length. Fig. 11 exemplifies the effect of changing the amplitude $f(0)$ while maintaining the decay length constant.

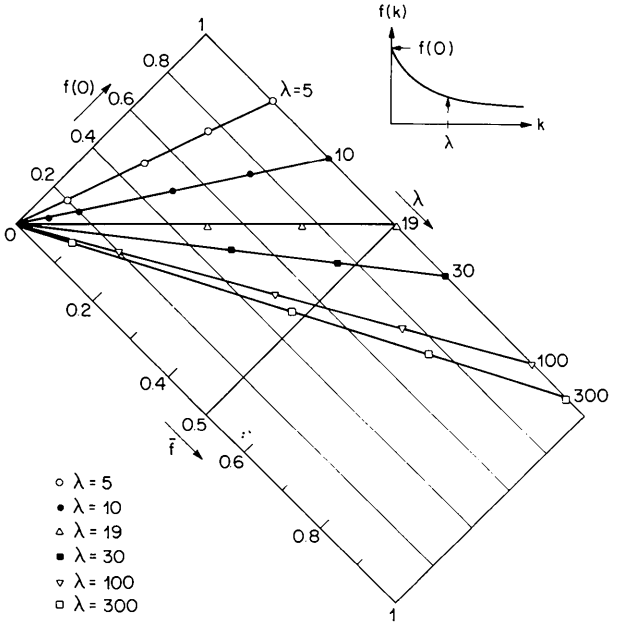

Fig. 9. Parameter-space map for position-dependent random stacking. The orientation of the map with respect to that of Fig. 1 is intended to highlight the fact that the introduction of a position-dependent abundance induces a tendency toward phase separation (see text). Thus, the $\bar{f}$ axis corresponds to the diagonal $p = (1 - q)$ in Fig. 1. The coordinates are a decay length, λ, and an amplitude, $f(0)$, both referring to an exponential profile; λ is measured in terms of number of layers. The average abundance, $\bar{f}$, is a function of λ and $f(0)$, and is given by (36). The map exhibits reflection symmetry with respect to the line $\bar{f} = \frac{1}{2}$. The contours of constant decay length, λ, were constructed on the basis of numerical evaluations of the scattering function for given $f(0)$ and λ, by plotting points $f(0)$, $\bar{f}$ corresponding to a chosen λ. As expected from (36), they are straight lines of slope $S_N(\lambda)/N$. The map was calculated for the 004 peak, with $N = 31$, $d_1 = 56{\cdot}5$ and $d_2 = 58{\cdot}9$ Å. The topography is expected to be independent of other choices of these system parameters. The inset illustrates an exponential abundance profile and serves to define $f(0)$ and λ; the index, k, numbers the layers in the stack.

6.3. *Non-stationary nearest-neighbor correlated stacking*

In § 2 we show that the general scattering function, (10), contains a contribution C_n if the first spacing is chosen with other than the stationary probability given in (5). As shown in (7), the effect of specifying

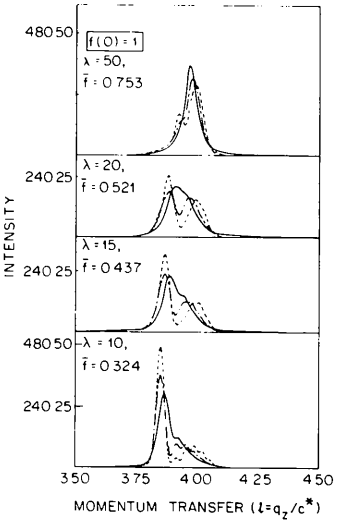

Fig. 10. Position-dependent random stacking. Exemplary line shapes of 004 peak in a system with parameters $N = 31$, $d_1 = 56{\cdot}5$ and $d_2 = 58{\cdot}9$ Å. These line shapes illustrate the effect of a changing penetration depth for exponential (——), Gaussian (— · —) and step (— — —) profiles.

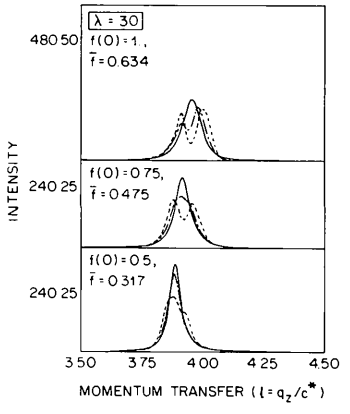

Fig. 11. Position-dependent random stacking. Exemplary line shapes of 004 peak in a system with parameters $N = 31$, $d_1 = 56{\cdot}5$ and $d_2 = 58{\cdot}9$ Å. These line shapes illustrate the effect of a changing amplitude for exponential (——), Gaussian (— · —) and step (— — —) profiles.

a 'boundary condition', $C_n \neq 0$, on the conditional probability for layer k to be type 1, given that layer 1 is type 1, decays by the geometric factor $(p+q-1)^{k-1}$. Therefore, the result of choosing other than the stationary probability for the first spacing can also be thought of as introducing a particular type of position-dependent average composition. The contribution of the C_n to $\langle I_N \rangle$ will be large only if both the correlation length associated with the non-vanishing C_n is comparable to N and also the magnitude of the departure from the stationary probability is of the order of 1. Both these criteria are met in Fig. 12, which illustrates the effect of C_n on $\langle I_N \rangle$ in a situation where $P_1(1)$ is chosen to equal zero, $(1-q)/(2-p-q)$, or unity. The C_n allow incorporation of this particular type of position-dependent composition in the nearest-neighbor correlated stacking model. For example, if one chooses $q = 1-p$, the expected composition in the resulting random stack will exhibit a geometric decline from the boundary, clearly equivalent to specifying $P_1(1) = f(0)$, and a geometric profile for $f(k)$ in the previously discussed position-dependent random stack.

6.4. *Constrained random stacking*

Another probabilistic rule for constructing an ensemble of stacks is obtained by constraining composition in random layer sequences. That is, one constrains the total number of spacings of type 1 to be J, and the remaining $(N-J)$ spacings to be of type 2, thereby adjusting the abundance of type 1 to be $f_1 = J/N$. All configurations are equally probable. This model may apply when some of the possible random stacks do not occur.

Equation (3) applies in this case, the probability density W_n^j being the hypergeometric distribution (Feller, 1968)

$$W_n^j = \binom{J}{j}\binom{N-J}{n-j}\Big/\binom{N}{n},$$

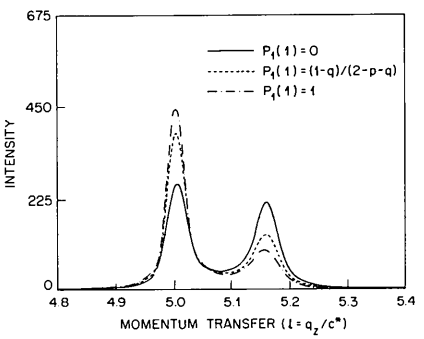

Fig. 12. Non-stationary nearest-neighbor correlated stacking. The examples illustrate the effect of specifying the initial probability, $P_1(1)$, to equal 0, $(1-q)/(2-p-q)$ and 1. The profiles were evaluated for the 005 maximum, with $N = 30$, $p = 0{\cdot}95$, $q = 0{\cdot}9$ and $d_1/d_2 = 31/32$, employing the full version of equation (10); $c^* = 2\pi/d_1$.

where $0 \leq j \leq J \leq N$, $0 \leq (n-j) \leq (N-J)$; W_n^j gives the probability that in a substack of length $n \leq N$, j spacings are of type 1. For $n > J$, W_n^j vanishes. As there is no k dependence, the sum over k in (3) contributes a multiplicative factor $(N-n)$; the B_n can be computed from (9).

In Fig. 13 we display the result of comparing random and constrained random stacks of the same composition. The normalized peak intensity $i_N = \langle \hat{I}_N \rangle / N^2$, plotted as a function of $(1-f_1) = f_2$, is seen to decrease more rapidly in random stacks. This is illustrated by two sets of plots, for $N = 30$ and $N = 100$. The general argument given in § 6.0, stating that the integrated intensity is of order N, applies to constrained random stacks. Hence, the composition dependence of $i_N^{CRS} \geq i_N^{RS}$ implies the integral peak width w^{CRS} of constrained stacks to be bounded by that of the corresponding random stack.

The inset to Fig. 13 contains two representative line shapes. The signal for the constrained stack displays characteristic oscillations. These are gradually smoothed as N becomes large ($N \gg J$) and the hypergeometric distribution approaches the binomial distribution. In accordance with the identity of the means of the two distributions, peak positions coincide. We note that the composition dependence of i_N satisfies an approximate scaling relation such that the function $i_{N_1}^{CRS}$ for a *constrained* stack of N_1 layers is well approximated by $i_{N_2}^{RS}$ for a *random* stack of $N_2 < N_1$. This is apparent from Fig. 13.

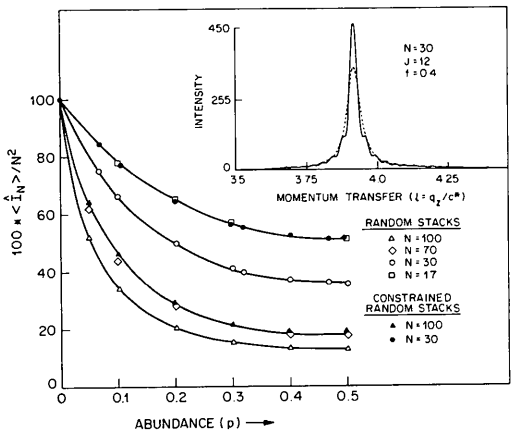

Fig. 13. Constrained random stacking. Shown is the decrease of the normalized peak height, $\langle \hat{I}_N \rangle / N^2$, of a constrained random stack (solid symbols) in comparison with that of a random stack (open symbols) of equal composition as a pure ($p = 0$) evolves into an equi-abundant ($p = 0{\cdot}5$) state. The behavior for two systems ($N = 30$, $N = 100$), with $d_1 = 56{\cdot}5$ and $d_2 = 58{\cdot}9$ Å is shown. Also indicated is the behavior of random stacks of reduced size approximating constrained random stacks. Corresponding pairs of random and constrained random stacks are: $N = 70$ and $N = 100$, as well as $N = 17$ and $N = 30$. The inset illustrates characteristic line shapes for a random (- - -) and a constrained random (——) stack of average abundance $f_1 = 0{\cdot}4$.

7. Summary and concluding remarks

In this paper we have presented a statistical analysis of X-ray scattering probing pure displacement disorder in one dimension in crystals containing two components and N unit cells, or layers. The analysis relies on a formulation of the scattering problem in terms of the probability distributions that prescribe the possible layer sequences. Given such a distribution, an appropriate ensemble average yields the scattering function. This formulation is sufficiently general to permit the treatment of a variety of types of one-dimensional disorder.

Detailed consideration was given to the important case in which layer sequences are determined by nearest-neighbor correlations. Specifically, if the layer sequence is specified as a Markov chain with nearest-neighbor transition, and random initial probabilities, complete eqivalence to the transfer matrix theory of Kakinoki & Komura obtains. This problem admits of explicit solution for the relevant generating function. This serves as a useful basis to rationalize and discuss the characteristics of the scattering function, in particular its line shape. An extensive exposition of such characteristic features was presented.

Motivated by recent experiments, we have also investigated cases of *non-stationary* transition probabilities, which reflect a spatially varying distribution of spacing in random sequence. The numerical evaluation of the appropriate ensemble average yields the scattering function throughout the parameter space pertaining to exponential, Gaussian, and stepped profiles of the relative abundance of spacings. The calculations reveal a tendency toward phase separation shared by all profiles. For given average abundance, this tendency is found to be least pronounced for the exponential. In contrast, a step profile induces almost complete segregation, thus closely mimicking nearest-neighbor correlated spacing with particular *stationary* transition probabilities.

The consequences of constraining composition fluctuations in randomly stacked layers have also been investigated. Comparison of resulting scattering functions with those generated by a random stack of equal average abundance reveals strikingly 'rippled' line shapes and a narrowing of the line width in the presence of the constraint. The latter may be rationalized in terms of the variances of the applicable probability distributions.

Mention has already been made of the relevance of the theory to the analysis of recent scattering experiments in which the adsorption of water into thin lyotropic multilayers was found to proceed *via* distinct states of hydration (Seul, 1988; Seul & Eisenberger, 1989).

The availability of results for non-stationary transition probabilities may also prove useful in the X-ray analysis of such problems as the penetration of a 'guest' species, deposited on a multilayer of a 'host' species of differing size. Such interdiffusion experiments have, for example, been considered for certain block copolymer systems.

Another field of interest for the potential applicability of our findings (Prost, personal communication) is that of 'frustrated' liquid-crystal phases. As Prost and collaborators have shown, a variety of novel smectic phases and new critical points arise in a theory of the polymorphism of polar liquid crystals, which considers smectic ordering with one of two possible incommensurate wave vectors, $|\mathbf{k}_1| = 2\pi/d_1$ and $|\mathbf{k}_2| = 2\pi/d_2$ (Prost & Barois, 1983; Barois, Prost & Lubensky, 1985). The informed examination by X-ray scattering of binary mixtures of appropriate components, the choice of relative sizes permitting the adjustment of the incommensurability, would certainly be facilitated by the understanding of the expected scattering line shapes.

MS acknowledges the hospitality of the Theoretical Biology and Biophysics Group at Los Alamos National Laboratory where part of this work was carried out. We thank Ms Patricia Reitemeier for preparing the manuscript.

APPENDIX *A*

We illustrate the derivation of the generating function for the probability ${}^1W_n^j$, which is used to derive (9).

First, the generating function ${}^1W(s, t)$ is defined by

$$ {}^1W(s,t) \equiv \sum_{n=1}^{\infty} t^{n-1} \sum_{j=0}^{n} {}^1W_n^j s^j. \qquad (A.1) $$

To derive a formula for ${}^1W(s, t)$, we introduce the probabilities ${}^1P_n^j$ (and ${}^1Q_n^j$) that the first layer is type 1 and that there are exactly j layers of type 1, and that the last layer is type 1 (type 2).

From (4), these probabilities obey the recursion

$$ {}^1P(j,n) = p\,{}^1P(j-1, n-1) + (1-q)\,{}^1Q(j-1, n-1) + \delta_{n-1}\delta_{j-1}, \qquad (A.2) $$

$$ {}^1Q(j,n) = q\,{}^1Q(j, n-1) + (1-p)\,{}^1P(j, n-1). \qquad (A.3) $$

Kronecker deltas appear in (*A*.2), specifying the initial layer is type 1. Use of the same rule to form the generating functions as given in (*A*.1) gives

$$ {}^1P(s,t) = pst\,{}^1P(s,t) + (1-q)st\,{}^1Q(s,t) + s, \qquad (A.4) $$

$$ {}^1Q(s,t) = qt\,{}^1Q(s,t) + (1-p)t\,{}^1P(s,t). \qquad (A.5) $$

These equations for ${}^1P(s, t)$ and ${}^1Q(s, t)$ are solved to give

$$ {}^1W(s,t) = {}^1P(s,t) + {}^1Q(s,t) = \frac{s(1-qt) + (1-p)st}{1-(ps+q)t-(1-p-q)st^2}. \qquad (A.6) $$

The same procedure gives

$$^2W(s,t)=\frac{1-pst+(1-q)st}{1-(ps+q)t-(1-p-q)st^2}. \qquad (A.7)$$

Summations over the index j which appear in (8) are accounted for if we set our variable s equal to $\exp[i(\varphi_1-\varphi_2)]$. To find the summands of index n appearing in (8) from the generating functions (A.6) and (A.7), one can factor the denominator into two terms using the quadratic formula, use partial fractions, and then the easily obtained coefficient of t^{n-1} is proportional to the summand. Although this approach is less direct than the eigenvalue method used by Kakinoki & Komura (1952, 1965), it affords additional insight into the meaning of the coefficients B_n and C_n that appear in (9) and (10).

APPENDIX *B*

The results of §§ 3-5 contain the formal solution to the problem of evaluating the scattering function, $\langle I_N\rangle$, defined in (3) for a one-dimensional crystal of N unit cells exhibiting pure displacement disorder and containing two components coupled by nearest-neighbor interactions. The dependence of these solutions on the parameters is made explicit in this Appendix.

First, consider the diffuse term, D. We introduce polar representations for $\mathrm{tr}\,\mathbf{Q}=\tau$ and $B_1=f_1E_1+f_2E_2=\gamma$, *i.e*

$$\tau=t\exp(-i\alpha) \qquad (B.1a)$$

with

$$t=|\tau|=[(p-q)^2+4pq\cos^2\tfrac{1}{2}(\varphi_1-\varphi_2)]^{1/2}, \qquad (B.1b)$$

$$\tan\alpha=\frac{p\sin\varphi_1+q\sin\varphi_2}{p\cos\varphi_1+q\cos\varphi_2}, \qquad (B.1c)$$

and

$$\gamma=g\exp(-i\beta), \qquad (B.2a)$$

with

$$g=|\gamma|=[(f_1-f_2)^2+4f_1f_2\cos^2\tfrac{1}{2}(\varphi_1-\varphi_2)]^{1/2}, \qquad (B.2b)$$

and

$$\tan\beta=\frac{f_1\sin\varphi_1+f_2\sin\varphi_2}{f_1\cos\varphi_1+f_2\cos\varphi_2}. \qquad (B.2c)$$

In (B.1b) and (B.2b), the phase difference $(\varphi_1-\varphi_2)$ may be written in terms of two spacings, d_1 and d_2, in the form $\varphi_1-\varphi_2=(2\pi/d_1)(d_1-d_2)l$, where l measures the normal component of the momentum transfer in units of $2\pi/d_1$. Now, the diffuse term of (26) becomes

$$D=(\Delta\Delta^*)^{-1}\{1+t^2+\lambda^2-2t\cos\alpha+2g\cos\beta -2gt\cos(\beta-\alpha)-2g\lambda\cos[\beta-(\varphi_1+\varphi_2)]\}, \qquad (B.3a)$$

where $\lambda=1-p-q$ is the negative of one of the eigenvalues of $\mathbf{P}$ and $\Delta=1-\tau-\lambda E_1E_2$ is the determinant of the matrix $\mathbf{I}-\mathbf{Q}$. The denominator of D is

$$\Delta\Delta^*=1+t^2+\lambda^2-2t\cos\alpha-2\lambda\cos(\varphi_1+\varphi_2) +2\lambda t\cos(\varphi_1+\varphi_2-\alpha). \qquad (B.3b)$$

Use of the polar representation given above for the variables occurring in H of (27) results in (30).

APPENDIX *C*

```
      program pdrs (tty, tape 1 = tty)
      real pr(ns)
      complex p(ns), b(ns)
      pi = 4. * atan(1.)
      ph1 = 2. * pi * x1
      ph2 = 2. * pi * x2
      do 10 i = 1,ns
      p(i) = cexp(cmplx(0.,phl)) * pr(i)
     + cexp(cmplx(0.,ph2)) * (1. - pr(i))
10    continue
      b(1) = cmplx(1.,0.)
      sigma = 0.
      do 20 i = 1,ns
      b(1) = b(1) * p(i)
20    continue
      sigma = real(b(1))
      do 40 n = ns - 1,1,-1
      b(ns + 1 - n) = b(ns - n)
      do 30 k = 1,ns - n
      b(k) = b(k)/p(k + n)
      sigma = sigma + real(b(k))
30    continue
      b(ns + 1 - n) = b(ns + 1 - n)/p(ns - n)
      sigma = sigma + real(b(ns + 1 - n))
40    continue
      xr = ns + 1. + 2. * sigma
      stop
      end
```

In this Fortran program *pdrs*, one must specify *ns*, the number of spacings; *x*1, the momentum transfer for a spacing of type 1; *x*2, the momentum transfer for a spacing of type 2; and the *ns* probabilities, pr(i), that spacing i is type 1. A description of the intrinsic functions used can be found in Appendix *B* of the Cray CFT77 reference manual, no. SR-0018. *xr* is the desired X-ray scattering intensity for a position-dependent random stack as given between (32) and (33), assuming $|V|^2$ equals unity.

References

BAROIS, P., PROST, J. & LUBENSKY, T. C. (1985). *J. Phys. (Paris)*, **46**, 391-399.

BARTLETT, M. S. (1978). *An Introduction to Stochastic Processes*, 3rd ed., ch. 2. Cambridge Univ. Press.

FELLER, W. (1968). *An Introduction to Probability Theory and Its Applications*, Vol. 1, 3rd ed., pp. 43, 432. New York: John Wiley.

GRIMM, H., AXE, J. D. & KRÖHNKE, C. (1982). *Phys. Rev. B*, **25**, 1709-1716.
GUINIER, A. (1958). *Bull. Soc. Fr. Minéral. Cristallogr.* **78**, 680-710.
GUINIER, A. (1963). *X-ray Diffraction in Crystals, Imperfect Crystals and Amorphous Bodies.* New York: Freeman.
HENDRICKS, S. & TELLER, E. (1942). *J. Chem. Phys.* **10**, 147-167.
HOSEMANN, R. & BAGCHI, S. N. (1954). *Phys. Rev.* **94**, 71-74.
HUANG, K. (1963). *Statistical Mechanics.* New York: Wiley.
HUSTER, M. E., HEINEY, P. A., CAJIPE, V. B. & FISCHER, J. E. (1987). *Phys. Rev. B*, **35**, 3311-3326.
JAGODZINSKI, H. (1987). *Prog. Cryst. Growth Charact.* **14**, 47-102.
JAMES, R. W. (1982), *The Optical Principles of the Diffraction of X-rays.* Woodbridge, CT: Ox Bow Press.
JOHNSTON, D. C. & FRYSINGER, S. P. (1984). *Phys. Rev. B*, **30**, 980-984.
KAKINOKI, J. (1967). *Acta Cryst.* **23**, 875-885.
KAKINOKI, J. (1983). *Acta. Cryst.* A**39**, 171-173.
KAKINOKI, J. & KOMURA, Y. (1952). *J. Phys. Soc. Jpn*, **7**, 30-35.
KAKINOKI, J. & KOMURA, Y. (1965). *Acta Cryst.* **19**, 137-147.
KASTELEYN, P. W. (1971). *Trieste Lectures* 1970. Vienna: International Atomic Energy Agency.
KIM, H. J., FISCHER, J. E., MCWHAN, D. B. & AXE, J. D. (1986). *Phys. Rev. B*, **33**, 1329-1339.
KOMURA, Y. & KITANO, Y. (1977). *Acta Cryst.* B**33**, 2496-2501.
LANDAU, L. (1937). *Phys. Z. Sowjetunion*, **12**, 579-585.
LIFSCHITZ, I. M. (1937). *Phys. Z. Sowjetunion*, **12**, 623-643.
LIFSCHITZ, I. M. (1939). *J. Exp. Theor. Phys. USSR*, **9**, 500-509.
MAIRE, J. & MÉRING, J. (1970). In *Chemistry and Physics of Carbon*, Vol. 6, edited by P. L. WALKER. New York: Marcel Dekker.
MÉRING, J. (1949). *Acta Cryst.* **2**, 371-377.
MONCTON, D. E., DISALVO, F. J., AXE, J. D., SHAM, L. J. & PATTON, B. R. (1976). *Phys. Rev. B*, **14**, 3432-3457.
PROST, J. & BAROIS, P. (1983). *J. Chim. Phys.* **80**, 65-81.
REYNOLDS, R. C. (1980). *Crystal Structures of Clay Minerals and Their X-ray Identification*, edited by G. W. BRINDLEY & G. BROWN. Mineral. Soc. Monogr. no. 5.
RIORDAN, J. (1968). *Combinatorial Identities.* New York: Wiley.
SEUL, M. (1988). *Phys. Rev. Lett.* **60**, 1150-1153.
SEUL, M. & EISENBERGER, P. (1989). *Phys. Rev. A.* In the press.
SLATER, L. J. (1960). *Confluent Hypergometric Functions.* Cambridge Univ. Press.
WELBERRY, T. R. (1985). *Rep. Prog. Phys.* **48**, 1543-1593.

Acta Cryst. (1989). A**45**, 396-409

X-ray Refinement of Protein Structures by Simulated Annealing: Test of the Method on Myohemerythrin

BY JOHN KURIYAN

Laboratory of Bioorganic Chemistry and Biochemistry, The Rockefeller University, 1230 York Avenue, New York, NY 10021, USA

AXEL T. BRÜNGER*

Howard Hughes Medical Institute, Department of Molecular Biophysics and Biochemistry, Yale University, New Haven, CT 06511, USA

MARTIN KARPLUS

Department of Chemistry, Harvard University, 12 Oxford Street, Cambridge, MA 02138, USA

AND WAYNE A. HENDRICKSON

Howard Hughes Medical Institute, Department of Biochemistry and Molecular Biophysics, Columbia University, 630 West 168th Street, New York, NY 10032, USA

(*Received* 23 *August* 1988; *accepted* 3 *January* 1989)

Abstract

The recently developed method of structure factor refinement by molecular dynamics with simulated annealing [Brünger, Kuriyan & Karplus (1987). *Science*, **235**, 458-460] is tested on the 118 residue protein myohemerythrin. A highly refined structure for this protein at 1·3/1·7 Å resolution has recently been published [Sheriff, Hendrickson & Smith (1987). *J. Mol. Biol.* **197**, 273-296]. This is compared with the results of simulated annealing refinement (with no manual intervention) starting from an earlier model for the protein from a stage in the refinement when conventional least-squares methods could not improve the structure. Simulated annealing reduces the *R* factor at 2·5 Å from 39 to 31%, with uniform temperature factors and no solvent molecules and with similar stereochemistry; the comparable value for the manually refined structure is 27·9%. Errors in backbone and sidechain positions up to about 3 Å are corrected by the method. The error in backbone positions for roughly 85% of the initial structure is within this range, and in these regions the r.m.s. backbone error is reduced from 1·1 to 0·4 Å. For the

0108-7673/89/060396-14$03.00